sciendo

Original Study   **Open Access**

Raksha Rani Sanadhya*, Jitendra Kumar Sharma, Ashish Solanki

Numerical Evaluation of Partially Strengthened Floating Granular Pile Raft With Vertical and Radial Displacement Compatibility

Abstract: In today's time, construction is the main key for development of any nation, but land resources are getting deplete. Thus, construction on compressible soil is left as a choice. Stone columns or granular piles (GPs) are broadly used to advance the bearing capacity of crummy ground and lessen the displacement of constructionserected on them. GP is the most efficient and cheap for ground improvement. Analysis of single partially strengthened (SPS) floating granular piled raft is presented in this paper in terms of several normalized aspects like vertical and radial displacement impact factors,settlement impact factor (SIF) for any depth, the normalized GP–soil interface shear and radial stresses, the load ratio, i.e., the percentage of the load taken by the GP and raft to the total load, and the normalized contact pressure distribution below the raft, which are evaluated for SPS floating granular piled raft. The SIF for top of GP is noticed to decline with the surge in the values of the strengthening parameters. The interfacial shear stresses get reorganized along the length of the GP.

Keywords: Floating GP; Settlement impact factor; Radial displacement impact factors; Comparative length of strengthening; Strengthening factor.

1 Introduction

In circumstances where a raft foundation solitary doesn't fill the plan demands, piles are added with raft to improveits performance, which is called a piled raft, where the piles are involved as settlement easer. Piled raft foundation system has been most particularly applied to high-rise buildings all over the world and progressively recognized as a relatively economical system for bridges and large-scale industrial plants. At the place of the conventional piled raft system of foundation, the piles are replaced with the granular pile (GP)/stone column, and in the present study, the GP is strengthened in the upper portion. Strengthening means the parent material of GP is replaced partially by constructing pile with the granular material (e.g., gravel, pebbles, or coarse dense sand) for better stiffness and strength. The strengthening in the upper portion of the pile is done to overcome the problem of bulging in the upper portion of the GP. Strengthening is represented through two variables, viz. one is for comparative length of strengthening of GP and other is for comparative strengthening of the upper portion to lower unstrengthened portion of the GP. The impact of the factors has been studied on the overall settlement, the lateral bulging of the GPs, and load distribution between raft, pile, and pile base. The outcomes showed that the GPs in compressible soil reduce the settlement and the lateral displacement of the GPs effectively. Additional improvements in the settlement of the raft and in the lateral displacement also occurred due to the increase of the strengthening parameters.

The effectiveness of piled rafts in improving the bearing capacity and minimizing the total and differential settlements was first proposed by Burland et al. [1]. Piled rafts systems were analyzed numerically, based on the boundary element method, the continuum approach, and simplified stiffness approach [2, 3]. The adoption of piled rafts is also related with economic and environmental aids: as reported by Huang et al.[4], the design tactic has been broadlyused in China, to the level that designing settlement-reducing piles for high buildings is presentlycompulsory in Shanghai. The cushion forbids loads approaching from the structure from being straightconveyed to the piles; hence, the separated piles function as soil reinforcements pretty than

*Corresponding author: Raksha Rani Sanadhya, Department of Civil Engineering, Rajasthan Technical University, Kota, E-mail: rrsanadhya.phd14@rtu.ac.in
Jitendra Kumar Sharma, Ashish Solanki, Department of Civil Engineering, Rajasthan Technical University, Kota

as pure structure members [5]. Liang et al. [6, 7] suggested that a cushion made with sand-gravel materials plays a vitalpart in activating the bearing capacity of the subsoil and in amending the load transmission mechanism of piles. Eslami and Malekshah [8] investigatedelasto-plastic analyses to demonstrate that the extreme axial stress along piles arises at different depths liable on the thickness and stiffness of the cushion. Tradigo et al. [9, 10] performed 3D finite element analyses to show that an increase in cushion thickness will reduce the overall settlement/stiffness. The settlement of the raft decreases with a surge in the length of the long piles [11]. Eid and Shehada [12] studied that having rock as the foundation subgrade expressively sinks the pile-load share and accordinglydeclines the proficiency of using long piles as foundation settlement reducers. An estimatedtactic with the idea of the interaction factor was employed by Maosong Huang et al. [13] to examine the nonlinear functioning of pile groups with a rigid cap. Fumio Kuwabara [14] concluded that the percentage of the long-term settlement to the total final settlement of pile groups was better than that of single piles. In piled rafts, this proportion was smaller than that in free-standing groups, but the effect of the raft is small except for short pile groups. Sungjune Lee and Joon-Shik Moon [15] found that the piles in a piled raft foundation reduce the total settlement also surge the total bearing capacity, it was proved to be vitalinapproximationprecisely the nonlinear functioning of piles after resilient for the fiscal design of piled raft foundation. Discrepancy of normalized settlement with soil rigidity under different factors of safety was endorsed by Ruping Luo et al. [16]. Maharaj et al. [17] stated that the corner pile gets its ultimate capacity at slightest settlement, trailed by the edge pile, and the center pile gets its ultimate capacity at higher settlement. Analysis of pile groups having a rigid cap in connection with the ground was studied by Shen et al. [18]. This paper is intended at examining the impact of the raft–soil–pile interactions on the load transfer mechanisms of the partially strengthened piled raft foundation system based on the continuum approach with radial displacement compatibility of GP. Mindlin's equations are used for computation of radial and vertical displacement within the elastic continuum. For normal stresses at the raft interface, Boussinesq's equations are numerically integrated for evaluating the radial and vertical displacement at any point within the elastic half-space. Displacement at the interface of strengthened and unstrengthened portions of GP is maintained through compatibility of displacements at the interface of strengthened and unstrengthened elements.
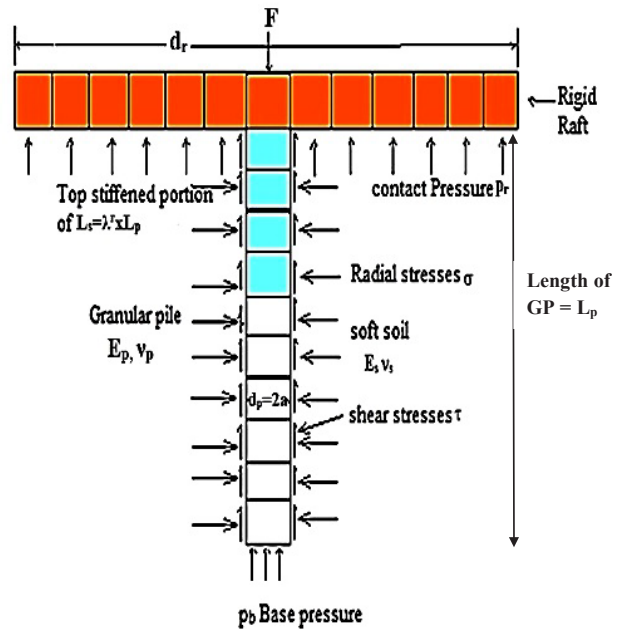

Figure 1: Force and stresses on a partially strengthened piled raft foundation.

2 Problem Definition

Partially strengthened floating granular piled raft foundation carrying an axial load F, with the length of GP, L_p, radius 'a', and diameter, d_p=2a, is shown in Fig. 1. The compressible soil is represented by the modulus of deformation, E_s, and Poisson's ratio, υ_s. The GP is compressible with the modulus of deformation, E_p, and Poisson's ratio, ν_p. The comparative strengthening of GP is defined as K_p= E_p/E_s, the ratio of deformation moduli of the GP to that of the soil. In the present analysis, it is assumed that the top portion of length L_s=λ^r×L_p has been strengthened where λ^r is constant for comparative length of strengthening of GP. The modulus of the deformation of the partially strengthened portion is E_{stp}. Comparative strengthening (K_{stp}) of the partially strengthened section of GP is μ^r times that of the unstrengthened portion, i.e., K_{stp} = $\mu^r K_p$, where μ^r is strengthening factor. It is assumed that the Poisson ratio ν_p is the same throughout the GP.

Mindlin's expressions for vertical and horizontal displacements due to both vertical and horizontal point loads acting within the soil mass are used to get vertical and radial soil displacements of GP. The pile is discretized into 'n' cylindrical element (segments), and each segment is additionally subdivided vertically into 'nz' and circumferentially into 'nt' segments and GP base is separated into 'nb' annular and 'nbt' angular subdivisions for numerical integration. The settlements for cylindrical

(a)   (b)

(c)
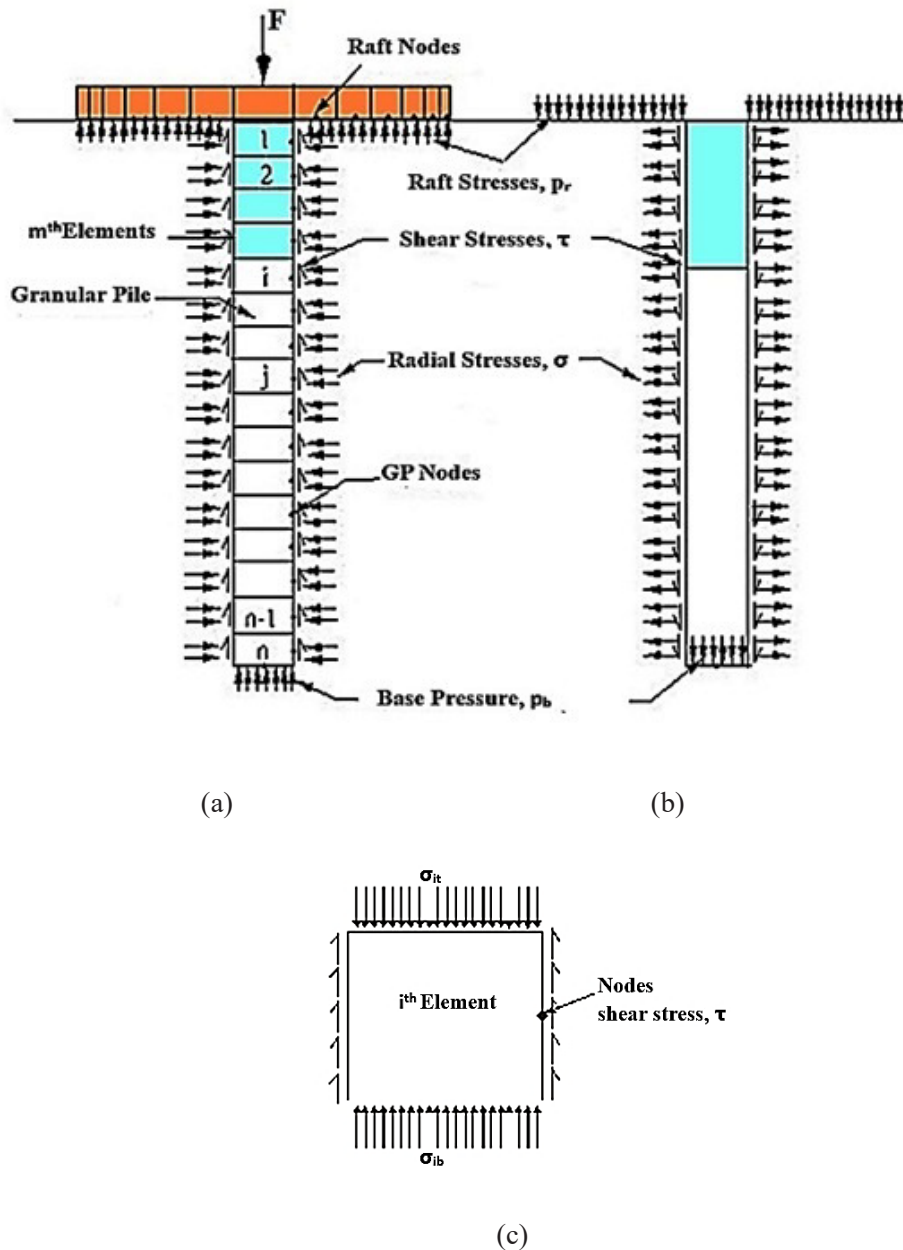
Figure 2: (a) Stresses on the GP and raft due to soil. (b) Stresses in the soil due to GP and raft. (c) Stresses on any i^{th} element of the GP.

segments are intended at the nodes at the periphery of each segment on the GP–soil interface, while for the base, the node is at the center of GP.

The raft is supposed to be rigid and of diameter, d_r. For mathematical integration, raft is discretized into 'kr' number of annular rings of equal areas. It is additionally subdivided into 'kt' number of angular subdivisions and 'τ' is the interface shear stresses between GP and soil, 'p_r'is the contact pressures at the raft–soil interface and 'p_b' is base pressure at pile tip as shown in Fig. 2. Settlement nodes are at the interfaces of soil and raft and the GP–soil interface.

3 Methodology

Mindlin's[19] and Boussinesq's solutions for a point load in the interior and on the surface of a semi-infinite elastic solid are adopted to calculate the displacement of soil at the interface of the soil and the pile and the soil and the raft, respectively. Following are the assumptions made in the analysis:

– The soil ishomogeneous, isotropic, and linearly elastic.
– The sides of GP are perfectly rough with no slip.

- GP base is supposed to be smooth and rigid.
- Stress-strain relationships of soil and GP material are linear.

3.1 Soil Displacement

Displacements along GP–soil interface are evaluated at the midpoint on the side of each element and at the center of the base by integration of Mindlin's and Boussinesq's expressions based on the influence of the elemental stresses of GP and the raft stresses, respectively, in matrix form following Sharma and Madhav [20].

$$\{\rho^{pv}\} = \left\{\frac{S^{pv}}{d_p}\right\} = [i^{vv}]\left\{\frac{\tau}{E_s}\right\} + [i^{vra}]\left\{\frac{\sigma_r}{E_s}\right\} + [i^{vr}]\left\{\frac{p_r}{E_s}\right\} \quad (1)$$

where $\{S^{pv}\}$ and $\{\rho^{pv}\}$ are vertical and normalized vertical soil settlement (VSS) vectors (superscript letters stand for 'p' pile, 'v' vertical shear stress, 'ra' radial stresses, and 'r' raft stresses), $[i^{vv}]$, $[i^{vra}]$, and $[i^{vr}]$ are matrix of size $(n+1)\times(n+1),(n+1)\times n$, and $(n+1)\times kr$, respectively, of the settlement impact factor (SIF), and $\{\tau\}$ and $\{p_r\}$ are column vectors of sizes $\{n+1\}$ and $\{kr\}$, respectively.

The radial displacements at midpoints of the elements and on the interface are

$$\{\rho^{pra}\} = \left\{\frac{S^{pra}}{d_p}\right\} = [i^{rav}]\left\{\frac{\tau}{E_s}\right\} + [i^{rara}]\left\{\frac{\sigma_r}{E_s}\right\} + [i^{rar}]\left\{\frac{p_r}{E_s}\right\} \quad (2)$$

where $\{S^{pra}\}$ and $\{\rho^{pra}\}$ are radial and normalized VSS vectors, and $[i^{rav}]$, $[i^{rara}]$, and $[i^{rar}]$ are matrix of size $n\times(n+1)$, $n\times n$, and $n\times kr$, respectively, of the SIF.

Displacements for soil–raft nodes are evaluated based on the interaction of elemental stresses from raft and GP. Soil displacement equations for raft nodes in matrix form are

$$\{\rho^r\} = \left\{\frac{S^r}{d_p}\right\} = [i^{rv}]\left\{\frac{\tau}{E_s}\right\} + [i^{rra}]\left\{\frac{\sigma_r}{E_s}\right\} + [i^{rr}]\left\{\frac{p_r}{E_s}\right\} \quad (3)$$

where $\{S^r\}$ and $\{\rho^r\}$ are vertical and normalized VSS vector, and $[i^{rv}]$, $[i^{rra}]$, and $[i^{rr}]$ are matrix of size $kr\times(n+1)$, $kr\times n$, and $kr\times kr$, respectively, of the SIF.

3.2 GP Displacement

Generalized stress-strain relation is utilized to evaluate the vertical and radial displacements of the components or elements of the GP as

$$\varepsilon_v = \frac{[\sigma_v - 2v_p\sigma_{rr}]}{E_p} \text{ and}$$

$$\varepsilon_\theta = \varepsilon_r = \frac{[\sigma_r - v_p(\sigma_r + \sigma_v)]}{E_p} \quad (4)$$

where ε_v, ε_q, and ε_r are, respectively, the axial, tangential, and radial strains of an element. σ_v and σ_r are the axial and radial stresses on the element, respectively.

3.3 Relationship Between Axial and Shear Stresses of GP

The axial load, F, applied at the top of the GP is resisted by the shear stresses, τ, along the pile and the base pressure, p_b, as

$$F = \sum_{j=1}^{j=(n)} \frac{\tau_j\pi d_p L_p}{n} + p_b\frac{\pi d_p^2}{4} \quad (5)$$

where 'n' is the number of components of GP.

The direct stress on an element 'i' is calculated by taking the average of the stresses on top of element σ_{it} and bottom of element σ_{ib},

$$\sigma_{vi} = \frac{\sigma_{it} + \sigma_{ib}}{2} = p_b + \sum_{j=(i+1)}^{j=n} \frac{4(L_p/d_p)\tau_j}{n} + \frac{2(L_p/d_p)\tau_i}{n} \quad (6)$$

The above equation relates the shear stresses to axial stresses along the surface of component and is deduced in matrix form as

$$\{\sigma_v\} = [A]\{\tau\} \quad (7)$$

where $\{\tau\}$ and $\{\sigma_v\}$ are columns vectors of shear stresses of size (n+1). Matrix [A] represents the relation between axial and shear stresses in an upper triangular square matrix of size (n+1) for each element along the pile length and at the base of pile.

$$[A] = \begin{bmatrix} \frac{2(L_p/d_p)}{n} & \frac{4(L_p/d_p)}{n} & \frac{4(L_p/d_p)}{n} & \frac{4(L_p/d_p)}{n} & - & - & - & - & 1 \\ 0 & \frac{2(L_p/d_p)}{n} & \frac{4(L_p/d_p)}{n} & \frac{4(L_p/d_p)}{n} & - & - & - & - & 1 \\ 0 & 0 & \frac{2(L_p/d_p)}{n} & \frac{4(L_p/d_p)}{n} & - & - & - & - & 1 \\ - & - & - & - & - & - & - & - & - \\ - & - & - & - & - & - & - & - & - \\ - & - & - & - & - & 0 & \frac{2(L_p/d_p)}{n} & \frac{4(L_p/d_p)}{n} & 1 \\ - & - & - & - & - & 0 & \frac{2(L_p/d_p)}{n} & 1 \\ - & - & - & - & - & - & 0 & 0 & 1 \end{bmatrix} \quad (8)$$

The vertical settlements of pile nodes on each component are calculated from the settlements of top of GP, ρ_t, to bottom component by considering the strain of each element successively.The settlement, ρ_i^p, of any element 'i' is obtained as

$$\rho_i^p = \rho_t - \sum_{j=1}^{j=(i-1)} \varepsilon_{vj} \frac{\Delta z}{d_p} - \varepsilon_{vi} \frac{\Delta z}{2d_p} \quad (9)$$

where ε_{vi} and ε_{vj} are the axial strains of ith and j^{th} elements, respectively.

To calculate the settlement of the base of GP, the strain at the base is

$$\varepsilon_b = -\frac{dS^p}{dz} = \frac{p_b}{E_p} \quad (10)$$

Using finite difference scheme with unequal intervals of spacing, the above equation is

$$\frac{4S_{n-1}^p - 36S_n^p + 32S_{n+1}^p}{12(\Delta z/d_p)} = -\frac{p_b}{E_p} \quad (11)$$

where S_{n-1}^p, S_n^p, and S_{n+1}^p are the settlements of elements n - 1, n, and n+1, respectively. Rewriting equation (18) in the normalized form, one gets

$$4\rho_{n-1}^p - 36\rho_n^p + 32\rho_{n+1}^p = -\frac{p_b}{E_p}\frac{12(L_p/d_p)}{n} \quad (12)$$

By putting the values of ρ_{n-1}^p and ρ_n^p from Eq. (9), and rearranging the terms, one gets

$$\rho_{n+1}^p = \rho_t - \sum_{j=1}^{j=m} \varepsilon_{vj}\frac{\Delta z}{d_p} - \sum_{j=m+1}^{j=(n-2)} \varepsilon_{vi}\frac{\Delta z}{d_p} - $$
$$- \frac{34}{32}\varepsilon_{v(n-1)}\frac{\Delta z}{d_p} - \frac{18}{32}\varepsilon_{vn}\frac{\Delta z}{d_p} - \frac{6}{32}\frac{(L/d)}{nK_p}\frac{p_b}{E_s} \quad (13)$$

In the above equation, for the calculation of ε_{vj}, $K_{stp} = E_{stp}/E_s$ comparative strengthening of strengthened portion with soil is taken, while for calculation of ε_{vi}, and other ε_{vn}, and $\varepsilon_{v(n-1)}$, $K_p = E_p/E_s$ comparative strengthening of unstrengthened portion with soil is considered.

Combining Eqs (9) and (13), the vertical settlements of GP are

$$\{\rho^{ppv}\} = \rho_t\{1\} + [B]\left\{\frac{\sigma_v}{E_s}\right\} + [C]\left\{\frac{\sigma_r}{E_s}\right\} \quad (14)$$

where [B] and [C] are lower triangular matrices of sizes (n+1)×(n+1) and(n+1) × (n), which are given by

$$[B] = \frac{(L_p/d_p)}{nK_p}\begin{bmatrix} \frac{-0.5}{\mu^r} & 0 & 0 & 0 & - & - & - & - & 0 \\ \frac{-1}{\mu^r} & \frac{-0.5}{\mu^r} & 0 & 0 & - & - & - & - & 0 \\ \frac{-1}{\mu^r} & \frac{-1}{\mu^r} & \frac{-0.5}{\mu^r} & 0 & - & - & - & - & - \\ - & - & - & - & - & - & - & - & - \\ - & - & - & - & - & - & - & - & - \\ \frac{-1}{} & \frac{-1}{} & - & - & - & - & - & -0.5 & 0 \\ -1 & -1 & - & - & - & - & - & \frac{34}{32} & -\frac{18}{32} & -\frac{6}{32} \end{bmatrix}$$

$$[C] = \frac{v_p(L_p/d_p)}{nK_p}\begin{bmatrix} \frac{1}{\mu^r} & 0 & 0 & 0 & - & - & - & - \\ \frac{2}{\mu^r} & \frac{1}{\mu^r} & 0 & 0 & - & - & - & - \\ \frac{2}{\mu^r} & \frac{2}{\mu^r} & \frac{1}{\mu^r} & 0 & - & - & - & - \\ - & - & - & - & - & - & - & - \\ - & - & - & - & - & - & - & - \\ - & - & - & - & - & - & - & - \\ 2 & 2 & - & - & - & - & - & 1 \\ 2 & 2 & - & - & - & \frac{68}{32} & \frac{36}{32} & 0 \end{bmatrix} \quad (15)$$

Here in matrix [B] and [C], K_{stp} will be replaced by $\mu^r \times K_p$ for top elements of GP to take into consideration of the effect of strengthening upto a depth $\lambda^r L_p/d_p$.

Using the shear and axial stresses relationship (Eq. 7), the vertical settlement of GP nodes in terms of shear stresses and radial stresses is

$$\{\rho^{ppv}\} = \rho_t\{1\} + [D]\left\{\frac{\tau}{E_s}\right\} + [C]\left\{\frac{\sigma_r}{E_s}\right\} \quad (16)$$

where [D] is a square matrix of size, (n+1) = [B] [A].

3.4 Radial GP Displacements

The radial displacements of nodes are calculated depending on stress-strain relationship for the axi-symmetric case as

$$\varepsilon_\theta = \frac{S^{ppr}}{a} = -\frac{[(1-\nu_p)\sigma_r - \nu_p\sigma_v]}{E_p} \qquad (17)$$

where ε_q, S^{ppr}, and a are the tangential strain, radial displacement, and radius of GP, respectively. The equation in normalized and matrix form is

$$\{\rho^{ppr}\} = \left\{\frac{S^{ppr}}{d_p}\right\} = [E]\left\{\frac{\sigma_v}{E_s}\right\} + [F]\left\{\frac{\sigma_r}{E_s}\right\} \qquad (18)$$

where [E] and [F] are the matrices of sizes n×(n+1) and n×n, respectively, and are

$$[E] = \frac{\nu_p}{2K_p}\begin{bmatrix} \frac{1}{\mu^r} & 0 & - & - & 0 \\ 0 & \frac{1}{\mu^r} & - & - & - \\ - & - & - & - & - \\ - & - & - & - & - \\ - & - & - & 1 & 0 \end{bmatrix}$$

$$[F] = -\frac{(1-\nu_p)}{2K_p}[U] \qquad (19)$$

where [U] is a unit matrix of size 'n'. The radial displacements of GP in terms of interfacial shear stresses of GP and soil (Eqs (7) and (18)) are

$$\{\rho^{ppr}\} = [G]\left\{\frac{\tau}{E_s}\right\} + [F]\left\{\frac{\sigma_r}{E_s}\right\} \qquad (20)$$

where [G] is a matrix of size n×(n+1) = [E][A].

3.5 Raft Settlements

Raft is considered as rigid and hence settlements of raft nodes are all equal. The settlement of the top of the GP (ρ_t) is equal to raft settlement and expressed as

$$\{\rho^{pr}\} = \rho_t\{1\} \qquad (21)$$

where $\{\rho^{pr}\}$ is the raft displacement vector of size 'kr'.

3.6 Compatibility of Settlements

Satisfying the compatibility of settlements for GP, raft, and soil, solutions are obtained in terms of shear and radial and raft stresses at the GP–soil and raft–soil interfaces, respectively. Applying the compatibility condition for vertical settlements of GP (Eqs (1) and (16))

$$\{\rho^{pv}\}=\{\rho^{ppv}\} \text{ or}$$

$$[AA]\left\{\frac{\tau}{E_s}\right\} + [BB]\left\{\frac{\sigma_r}{E_s}\right\} + [i^{vr}]\left\{\frac{p_r}{E_s}\right\} = \rho_t\{1\} \quad (22)$$

where $[AA]=[i^{vv}]-[D]$ of size (n+1)×(n+1) and $[BB]=[i^{vra}]-[C]$ of size (n+1)×n.

Satisfying compatibility of radial displacements of GP, i.e., equating Eqs (2) and (20)

$$[CC]\left\{\frac{\tau}{E_s}\right\} + [DD]\left\{\frac{\sigma_r}{E_s}\right\} + [i^{rar}]\left\{\frac{p_r}{E_s}\right\} = \{0\} \quad (23)$$

where $[CC]=[i^{rav}]-[G]$ is of size n×(n+1) and $[DD]=[i^{rara}]-[F]$ is of size n×n.

For the compatibility of displacements of the raft (Eqs (3) and (21))

$$\{\rho^r\} = \{\rho^{pr}\}\text{or}$$

$$[i^{rv}]\left\{\frac{\tau}{E_s}\right\} + [i^{rra}]\left\{\frac{\sigma_r}{E_s}\right\} + [i^{rr}]\left\{\frac{p_r}{E_s}\right\} = \rho_t\{1\} \quad (24)$$

Simultaneous equations (29), (30), and (31) are solved to obtain the interfacial shear and radial stresses along GP with raft stresses at raft–soil interface. Finally, the displacements of raft and GP nodes are obtained.

$$S^p = \frac{F}{E_s d_p} i_p \qquad (25)$$

where i_p is SIF; under the axial load 'F' on partially strengthened granular piled raft, the settlement along the length of GP is calculated in terms of settlement influence factor (SIF), linked with other parameters μ^r, λ^r, and K_p.

Under the axial load 'F' on partially strengthened granular piled raft, the SIF for any depth, i_{pd}, is also defined as

$$S^{pd} = \frac{F}{E_s d_p} i_{pd} \qquad (26)$$

where i_{pd} is SIF for any depth z of GP.

Similarly the radial displacement of GP at any depth can be expressed as

$$U_r = \frac{F}{E_s d_p} i_r \qquad (27)$$

where i_r is radial displacement impact factor.

Results are evaluated and discussed in terms of following parameters to quantify the effect of strengthening the GP.

Parameter μ^r strengthening factor is defined as follows:

$$\mu^r = K_{stp}/K_p \qquad (28)$$

Parameter λ^r comparative length of strengthening is defined as follows:

$$\lambda^r = L_s/L_p \qquad (29)$$

All the parameters defined above are for partially strengthened GP having $\mu^r > 1$. If $\mu^r = 1$, they can be obtained for unstrengthened GP. The overall response of partially strengthened floating granular piled raft foundation is evaluated in terms of the vertical and radial displacement impact factors, the SIF for any depth, the normalized GP–soil interface shear and radial stresses, the load ratio, i.e., the percentage of the load taken by the GP to the total load, and the normalized contact pressure distribution below the raft. The parameters affecting the overall responses are (i) the geometric ones – the ratio of diameter of the raft to that of GP, i.e., diameter ratio, (d_r/d_p), and the length to diameter ratio of GP, (L_p/d_p); (ii) comparative GP–soil stiffness, i.e., $K_p = (E_p/E_s)$; (iii) Poisson's ratio of the soil, ν_s; (iv) strengthening factor $\mu^r = K_{stp}/K_p$ where $K_{stp} = (E_{stp}/E_p)$ and $K_p = (E_p/E_s)$; and (v) comparative length of strengthening of GP, λ^r.

4 Results and Discussion

Results obtained in this analysis have been validated with those of Madhav et al. (2009) for rigid raft on a single compressible unstrengthened floating pile analyses with or without radial displacement compatibility for radial displacement. The agreement has been very close as shown in Fig. 9. Results are obtained for the following ranges of non dimensional parameters, comparative length of GP, L_p/d_p = 10–30, comparative strengthening, K_p of GP

= 10–1000, comparative size of raft, d_r/d_p = 2–5, stiffness factor μ^r =1–10, and comparative length of strengthening from top of GP, λ^r = 0.1–0.4. Effect of Poisson's ratios of surrounding soil and GP does not affect the results significantly. Although the realistic normal range of K_p for GP are 10–100, results are obtained for K_p= 1000.

In order to compare the values of SIFs, i_p, obtained with and without satisfying radial displacement compatibility of nodes along GP, the variation of i_p with comparative GP–soil stiffness, with K_p, is shown in Fig. 3. For d_r/d_p=3, L_p/d_p=10, λ^r=0.4, and μ^r = 1, 2, 5, and 10, the value of SIF without radial compatibility and with radial compatibility are 0.227, 0.211, 0.194, and 0.185 and 0.224, 0.210, 0.193, and 0.184, respectively. The differences in the values of i_p obtained from the two analyses are in the range of 1–1.5% and decrease with the increase of strengthening factor μ^r. Thus, the consideration of radial displacement compatibility of GP in the analysis does not influence the SIF significantly.

Fig. 4 shows the effect of considering radial compatibility of displacement, on the value of SIF for top, i_p, it is quite clear from Fig. 3 that as by considering the radial compatibility, increases, SIF for top, i_p, decreases for all the values of comparative strengthening of GP, K_p. The increase in SIF is not significant because the percentage increase is only 1–2% at μ^r=1. The difference in the value of SIF is reducing with the increase in stiffness factor, μ, and comparative strengthening factor of GP, K_p. It can be seen as an illustration that for a partially strengthened granular piled raft, with L_p/d_p=10, d_r/d_p=3 with λ^r=0.4 and K_p=10, 50, 100, and 1000 with radial and without radial compatibility are 0.224, 0.178, 0.160, and 0.133 and 0.227, 0.176, 0.158, and 0.134, respectively. The effect of stiffness factor, μ^r, can also be seen that as it increases, the SIF for top, i_p, decreases because strengthening effect is enhancing.

Fig. 5 shows the effect of comparative length of strengthening, λ^r, from top of GP on SIF for top, i_p, for comparative size of raft, d_r/d_p=3 and 5 with considering the radial compatibility of displacement. With the increase in length of strengthening from top of GP, the SIF decreases. For example, a look at the graph reveals that for a partially strengthened granular piled raft with L_p/d_p=10, K_p=10, d_r/d_p=3, and λ^r= 0.2, 0.3, and 0.4, the values of i_p are 0.210, 0.202, and 0.197, respectively, hence causing a percentage decrease in value of about 3.8 and 6.1, respectively, showing the aspects of percentage length of strengthening by reducing the SIF for top, i_p.

Fig. 6 presents the variations of top SIF with the comparative strengthening of GP for L_p/d_p=10, with comparative length of strengthening from top of GP, λ^r=
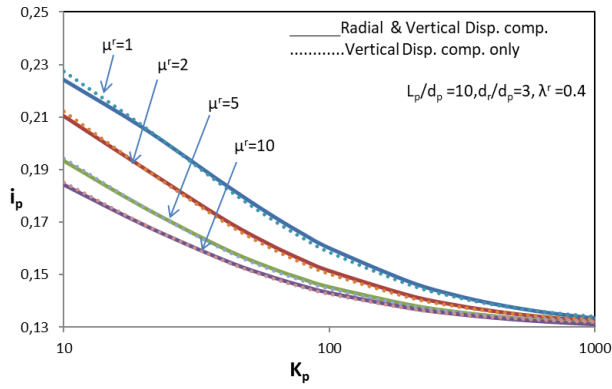
Figure 3: Variation of SIF, i_p, with comparative strengthening, K_p, of GP– effect of strengthening factor, μ^r, and radial and vertical settlement compatibility on partially strengthened GP–raft foundation ($L_p/d_p =10$, $d_r/d_p=3$, $\lambda^r =0.4$).
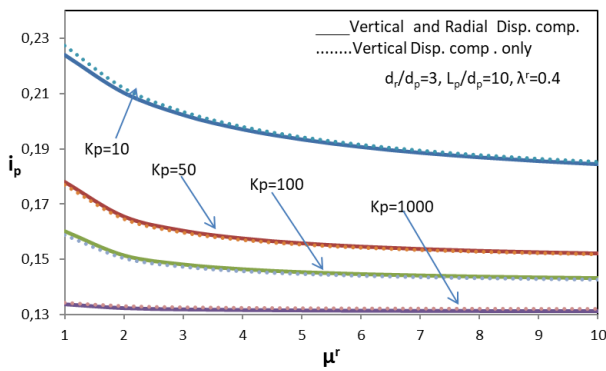
Figure 4: Variation of SIF, i_p, with comparative strengthening, μ^r, of GP– effect of comparative length of strengthening, K_p, of GP and radial and vertical settlement compatibility on partially strengthened GP–raft foundation ($L_p/d_p =10$, $d_r/d_p=3$, $\lambda^r =4$).
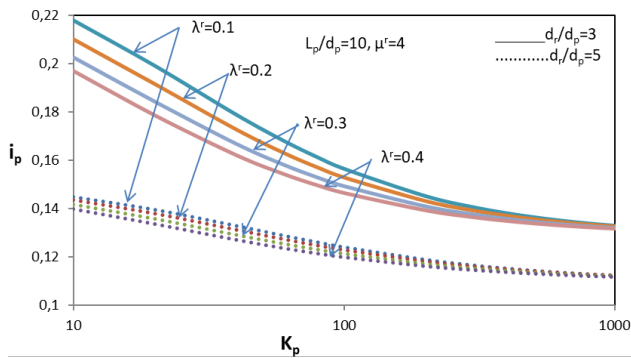
Figure 5: Variation of SIF, i_p, considering radial displacement with comparative strengthening, K_p, of GP– effect of comparative length, λ^r, of strengthening from top of GP and comparative size of raft, d_r/d_p, on partially strengthened GP–raft foundation ($L_p/d_p =10$, $\mu^r =4$).

0.4, stiffness factor, $\mu^r=1$, 5, and 10, and comparative size of raft, $d_r/d_p=3$ and 5. As expected, the SIF, i_p, decreases with the increase in the value of comparative strengthening, K_p, of GP. The SIF for single GP decreases from about 0.224 for homogeneous or unstrengthened GP ($\mu=1$) at $K_p = 10$, and $d_r/d_p=3$, to about 0.193 and 0.184 for μ^r equal to 5 and 10, respectively. The percentage reduction in the SIF, i_p, from $\mu^r=1$ to 5 is 13.8 and from $\mu^r=1$ to 10 is 17.8. It is also observed that as stiffness factor, μ^r, increases, the value of SIF, i_p, decreases showing the effect of strengthening. This occurs due to the stiffer portion of GP transferring the stresses toward the lower portion and the base of the GP. The rate of decrease of SIF, I_p, reduces with the increase in comparative size of raft from $d_r/d_p= 3$–5.

Fig. 7 shows the variation of SIF, i_p, with comparative strengthening, K_p, of GP with the effect of strengthening factor, μ^r, for $L_p/d_p =10$, $d_r/d_p=3$, and $\mu^r= 1$ and 5. The SIF, i_p, decreases with increase in the strengthening factor, μ^r. The value of i_p at $L_p/d_p =10$, $K_p=10$, $\lambda^r = 0.4$, and $d_r/d_p=3$ is about 0.224 for $\mu=1$ and the corresponding value for $\mu^r=5$ is 0.193 with percentage decreases of 13.8%. It is also noticed that SIF decreases with the increase of comparative strengthening of GP, K_p.

The influence of comparative length, L_p/d_p, of GP on the variation of SIF, i_p, with comparative strengthening of GP, K_p, is shown in Fig. 8 for $\mu^r = 1$ and 5. The SIF decreases with the increases of stiffness factor, μ^r. For $L_p/d_p= 10$ and $K_p = 10$, i_p decreases from 0.224 to 0.193 for μ^r increasing from 1 to 5. The values of i_p for $K_p = 10$, $\mu^r=5$, and $L_p/d_p =10$, 20, and 30 are 0.193, 0.175, and 0.168, respectively. The percentage decreases in SIF, i_p, are 9.3 and 12.9 for increases in L_p/d_p from 10 to 20 and from 20 to 30, respectively. The rate of decrease of SIF, i_p, decreases with K_p and with increase in comparative length, L_p/d_p.

Fig. 9 shows the influence of strengthening factor on radial displacement impact factor, i_r, for $d_r/d_p= 2$, 3, and 5. The increase of strengthening factor, μ^r, from 1 to 5 increases the radial displacement impact factor, i_r, and decreases along the depth of GP which shows the effect of strengthening in upper part. For strengthening factor, $\mu^r =1$ (unstrengthened) GP, the results are validated with the Madhav et al. [21] and found the variation trends are same. With the increase in comparative size of raft, d_r/d_p, the radial displacement impact factor, i_r, decreases at the top. The influence of normal stresses from raft on radial displacements of GP depends on their magnitude and comparative distances from the GP. Therefore, the maximum radial displacements of GP decrease and shift downward with the increase of d_r/d_p due to increase in load carried by raft, resulting in an increase in the confinement effect of raft. The radial displacement influence factor, i_r,
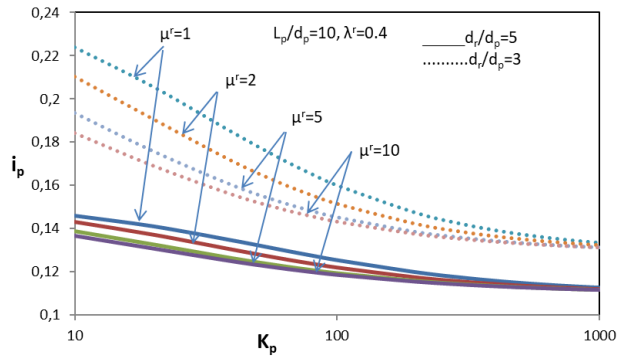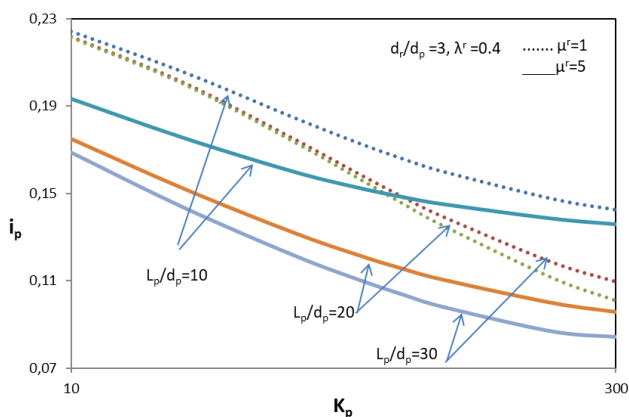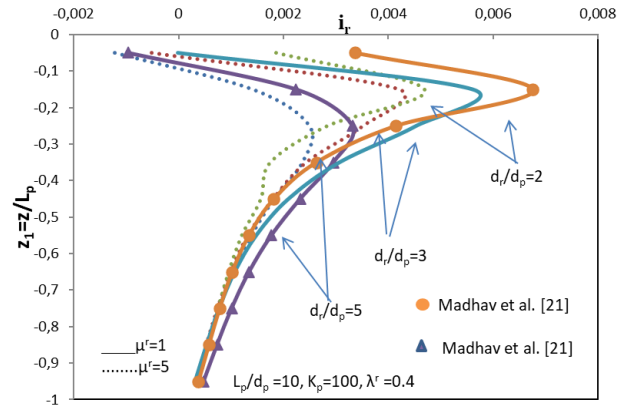
Figure 6: Variation of SIF, i_p, considering radial displacement with comparative strengthening, K_p, of GP– effect of strengthening factor, μ^r, and comparative size of raft, d_r/d_p, on partially strengthened GP–raft foundation (L_p/d_p =10, λ^r =0.4).
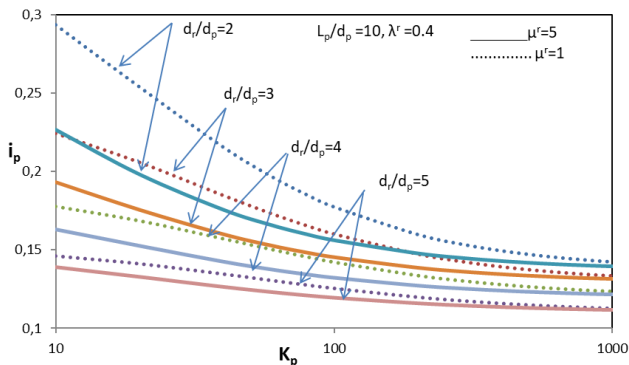
Figure 7: Variation of SIF, i_p, considering radial displacement with comparative strengthening, K_p, of GP– effect of comparative size of raft, d_r/d_p, and stiffness factor, μ^r, on partially strengthened GP–raft foundation (L_p/d_p =10, λ^r =0.4).

Figure 8: Variation of SIF, i_p, considering radial displacement with comparative strengthening, K_p, of GP– effect of comparative length of GP, L_p/d_p, and stiffness factor, μ^r, on partially strengthened GP–raft foundation (d_r/d_p =3, λ^r =0.4).


Figure 9: Variation of radial displacement impact factor, i_r, with comparative length of pile $z_1 = z/L_p$– effect of strengthening factor μ^r and comparative size of raft, d_r/d_p, and radial and vertical settlement compatibility on partially strengthened GP–raft foundation (L_p/d_p =10, K_p =100, λ^r =0.4).

decreases with the increase of comparative size of raft, d_r/d_p, except in the lower region of GP where it increases as shown in Fig. 9.

The radial displacement influence factor, i_r of GP, decreases along its depth with the increase of comparative strengthening of GP, K_p, as shown in Fig 10.This decrement in i_r with K_p is more for relatively smaller value of strengthening factor (μ^r=1) as compared to the reduction in case of larger one (μ^r=5). The maximum value of i_r for μ^r=1 is observed at a depth of 0.25L and its value decreases from 0.0033 for K_p = 50 to 0.0027 for μ^r=5. The percentage decrease in radial displacement impact factor, i_p, is 18.18 for increase in μ^r from 1 to 5.

The variation of radial displacement influence factor, i_r, with normalized depth, $z_1 = (z/L_p)$, is shown in Fig.11 for comparative length ofstrengthening, λ^r, of GP ranging from 0.2 to 0.4 and for L_p/d_p = 10. The radial displacement influence factor, i_r, increases at the top and decreases continuously with the depth of GP for the comparative length of strengthening, λ^r, in the range of 0.2–0.4. The values of radial displacement influence factor, i_r, decrease from 0.0041 to 0.0035 at z_1=0.25 for L_p/d_p=10, d_r/d_p=3, μ^r=4, K_p=100 with the increases of λ^r=0.2–0.4, and the percentage decrease in radial displacement influence factor, i_r, is around 17.14% which shows the effect of strengthening.

Fig. 12 clearly shows that due to increases in the value of comparative strengthening of GP, K_p, overall the values of τ^* decrease. The effect of strengthening factor, μ^r, can also be seen that as it increases, the shear stresses, τ^*, increase because strengthening effect is enhancing. It may be seen as an example that for partially strengthened floating granular piled raft with L_p/d_p=10, K_p=100, d_r/d_p=3,
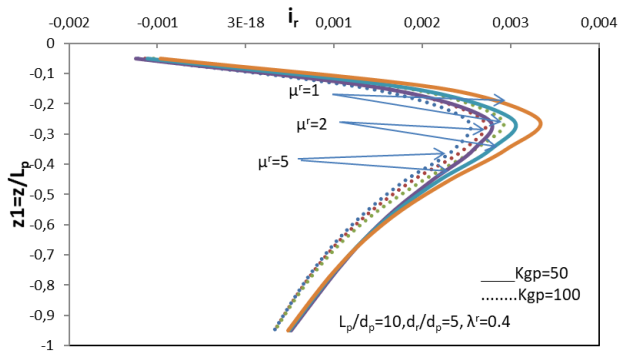
Figure 10: Variation of radial SIF, i_r, with the normalized depth, $z_1=z/L_p$ – effect of comparativestrengthening, K_p, of GP and strengthening factor, μ^r, on a partially strengthened GP–raft foundation ($L_p/d_p=10, d_r/d_p=5, \lambda^r=0.4$).
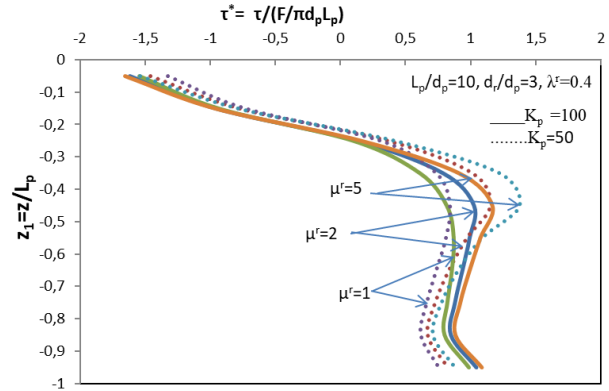

Figure 12: Variation of normalized shear stresses, $\tau^*= \tau/(F/\pi d_p L_p)$, with radial compatibility of the normalized depth, $z_1=z/L_p$ – effect of stiffness factor, μ^r, and comparative strengthening, K_p, of GP on a partially strengthened GP–raft foundation ($L_p/d_p=10$, $d_r/d_p=5$, $\lambda^r=4$).
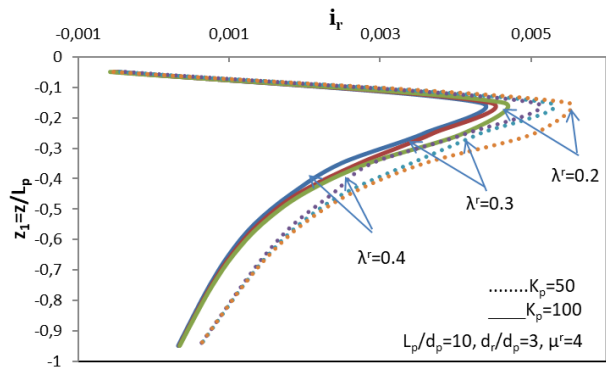
Figure 11: Variation of radial SIF, i_r, with the normalized depth, $z_1=z/L_p$ – effect of comparative strengthening, K_p, of GP and comparativelength of strengthening, λ^r, on a partially strengthened GP–raft foundation ($L_p/d_p=10$, $d_r/d_p=3$, $\mu^r=4$).
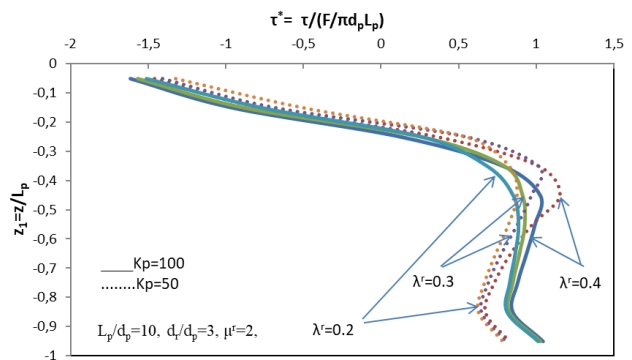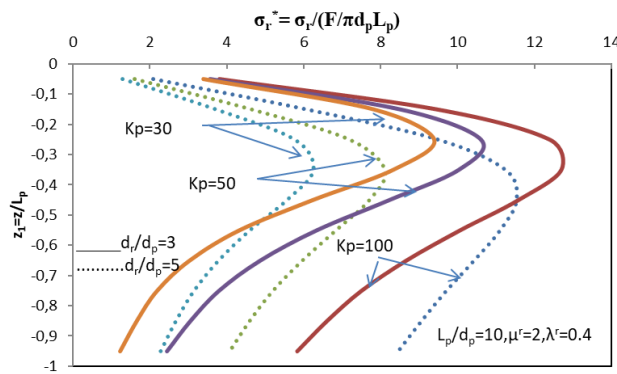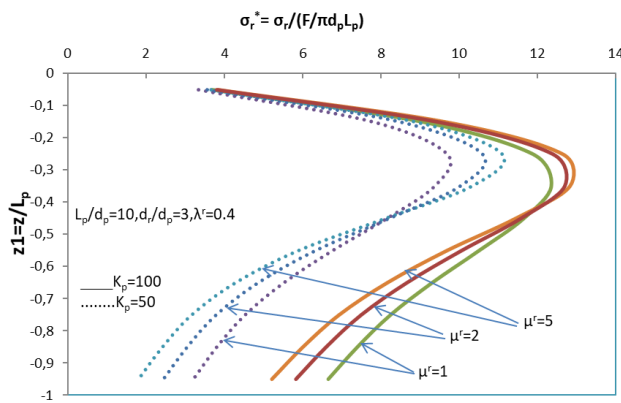

Figure 13: Variation of normalized shear stresses, $\tau^*= \tau/(F/\pi d_p L_p)$, with radial compatibility of the normalized depth, $z_1=z/L_p$ – effect of stiffness factor, μ, and comparative strengthening, K_p, of GP on a partially strengthened GP–raft foundation ($L_p/d_p=10$, $d_r/d_p=3, \mu^r=2$).

$\lambda^r=0.4$, and $\mu^r=1$, 2, and 5, the value of τ^* at $z_1=0.45$ are 0.81, 1.02, and 1.16, respectively.

Fig. 13 clearly shows that as comparativelength of strengthening, λ^r, increases, the normalized shear stresses increase. It is well noted that shear stresses are negative in upper part due to raft above the pile. The interfacial shear stresses upto length $z_1=0.25$ are negative, while in lower portion, stress becomes positive and goes on increasing. For $L_p/d_p=10$, $\mu^r=2$, $d_r/d_p=3$, $K_p=100$, and $\lambda^r=0.2$, 0.3, and 0.4 at $z_1=0.45$, the values of $\tau^*= \tau(\pi d_p L_p)/F$ are 0.85, 0.91, and 1.02, respectively, hence causing a percentage increase of 7 and 20. It can be seen as the shear stresses increase very steeply with the depth upto the comparative length of strengthening, $\lambda^r=0.4$, with the comparative strengthening of GP, K_p, these stresses are redistributed in lower portion of GP.

The variations of radial stresses on GP, i.e., $\sigma_r^*(\sigma_r/(F/\pi d_p L_p))$, with normalized depth of GP, $z_1= (z/L_p)$, are

shown in Fig. 14, showing the effect of comparative size of raft, d_r/d_p, and comparative strengthening of GP, K_p. The increase of d_r/d_p from 3 to 5 the radial stresses along the depth of GP decreases upto the length of $z_1=0.55$ after that radial stresses are increases due to normal stresses underneath the raft provide the confinement effect to GP decrease.With the increase of K_p, the radial stresses on GP increase along its depth. The effect of K_p on the radial stress distribution for comparative size of raft $d_r/d_p = 3$ is very similar to that obtained for $d_r/d_p = 5$ except that they decrease slightly with the increase of K_p in the top region of GP in the former case.

The variations of radial stresses normalized with the total load on GP, i.e., $\sigma_r^*= \sigma_r (\pi d_p L_p)/F$, with normalized depth of GP, $z_1= (z/L_p)$, are shown in Fig. 15, showing the influence of strengthening factor, μ^r. The radial stresses of GP increase upto the depth of strengthening in the range
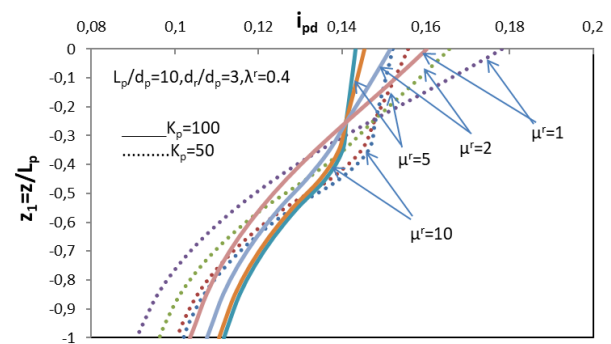
Figure 14: Variation of normalized radial stresses, $\sigma_r{}^* = \sigma_r\,(\pi d_p L_p)/F$, with the normalized depth, $z_1 = z/L_p$ – effect of stiffness factor, μ^r, and comparative strengthening, K_p, of GP on a partially strengthened GP–raft foundation ($L_p/d_p = 10$, $\mu^r = 2$, $\lambda^r = 0.4$).

Figure 15: Variation of normalized radial stresses, $\sigma_r{}^* = \sigma_r\,(\pi d_p L_p)/F$, with the normalized depth, $z_1 = z/L_p$ – effect of stiffness factor, μ^r, and comparative strengthening, K_p, of GP on a partially strengthened GP–raft foundation ($L_p/d_p = 10$, $d_r/d_p = 3$, $\lambda^r = 0.4$).

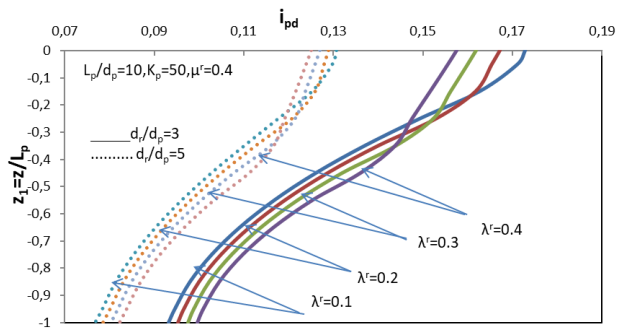**Figure 16:** Variation of SIF for any depth, i_{pd}, with normalized depth, $z_1 = z/L_p$ –effect of stiffness factor, μ^r, on homogeneous GP–raft and partially strengthened GP–raft ($L_p/d_p = 10$, $d_r/d_p = 3$, $\lambda^r = 0.4$).

$z_1 = 0$–4, and after that, they decrease with depth $z_1 > 4$. With the increase in stiffness factor, μ, the radial stresses on GP increase along with its depth of strengthening and redistributed in lower part of pile. This result follows from the increase in the load carrying capacity of upper stiffer part is increased GP with the increase of GP stiffness and capacity of lower unstrengthened part remaining constant.

Fig.16 shows the variation of SIF, i_{pd}, of a GP with normalized depth, $z_1 = z/L_p$, for unstrengthened and strengthened GPs with raft for $L_p/d_p = 10$, $K_p = 100$, $d_r/d_p = 3$, and $\lambda^r = 0.4$. Compatibility displacements at the interface of strengthened and unstrengthened portions of the GP are well satisfied. As strengthening factor, μ^r, changes from unstrengthened condition of GP, i.e., with $\mu^r = 1$ to strengthened condition with $\mu^r = 2$, 5, and 10, the SIFs, i_{pd}, for top are, respectively, 0.160, 0.151, 0.145, and 0.143. The

percentage decrease of settlement is 5.62, 9.37, and 10.62 showing the effect of strengthening. The rate of decrease of SIF decreases with increase in the strengthening of pile at the top.

The variation of SIF, i_{pd}, of a GP with normalized depth, $z_1 = z/L_p$, is shown in Fig.17 with the effect of comparative length λ^r of strengthening from top of GP for $L_p/d_p = 10$, $K_p = 50$, $d_r/d_p = 3$, and $\mu^r = 4$. For comparative length of strengthening from top of GP, $\lambda^r = 0.1$, 0.2, 0.3, and 0.4, the values of SIF, i_{pd}, for top are, respectively, 0.172, 0.167, 0.161, and 0.157 forpercentage decreases of 2.9, 6.3, and 8.7. SIF, i_{pd}, decreases rapidly with depth in the lower region, i.e., in unstrengthened portion of GP. For higher value of λ, the value of i_{pd} is maximum due to stresses transferred to the base with the length of strengthening.

Variations of contact pressures, $p_r{}^\star = (F_r/q)$, with normalized distance from the center of raft $R^\star = r/d_p$, with stiffness factor, μ^r. Effects of vertical and radial compatibility of displacement on a strengthened GP raft and raft alone are shown in Fig.18. The contact pressure distribution pattern for partially strengthened piled raft is very similar to that of the raft alone with the normal stress beneath a rigid raft increasing with distance from the center and tending to very high values at the edge of the raft. The percentage reductions in the contact pressure for $L_p/d_p = 10$, $d_r/d_p = 3$, $K_p = 50$, and $\mu^r = 10$ for vertical and considering radial with vertical compatibility in comparison to the value for a solid raft are, respectively, 23.28% and 14.28% near the edge of raft.

The contact pressure distribution at the raft–soil interface, $pr^\star = (F_r/q)$, with normalized distance from the center of raft, $R^\star = r/d_p$, can be seen in Fig. 19 for $L_p/d_p = 10$, $\mu^r = 4$, $\lambda^r = 0.4$, and $d_r/d_p = 3$ and 5. The percentage reduction in contact pressure for $K_p = 50$ and 100 for $d_r/d_p = 3$ and 5 in comparison to the values for $K_p = 30$ are 8.6% and 21.7% near the pile and 5% and 15% at the edge of pile,

Figure 17: Variation of SIF for any depth, i_{pd}, with normalized depth, $z_1 = z/L_p$ – effect of comparative length λ^r of strengthening from top of GP on partially strengthened GP–raft foundation ($L_p/d_p = 10$, $K_p = 50$, $\mu^r = 0.4$).
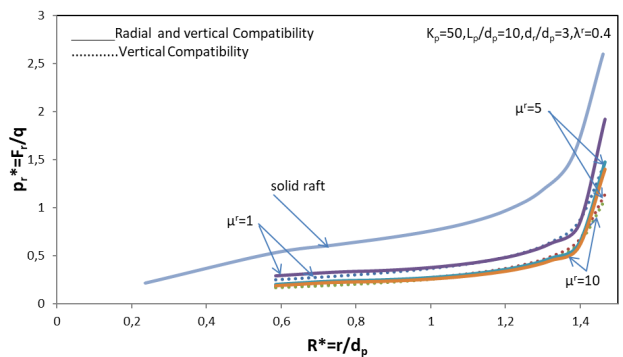
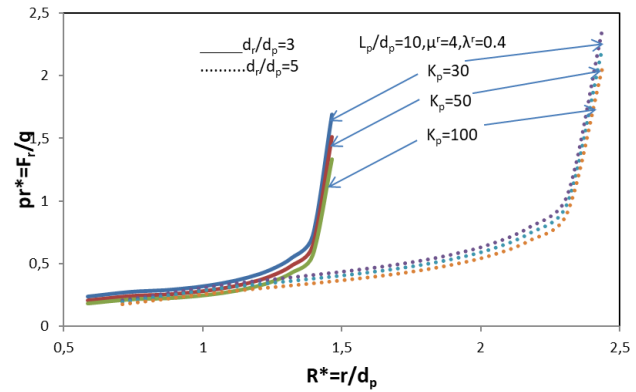
Figure 18: Variation of contact pressure ($p_r^* = F_r/q$) with normalized distance from the center of raft $R^* = r/d_p$ –effect of strengthening factor, μ^r, and vertical and radial compatibility of displacement on a partially strengthened GP–raft and solid raft ($K_p = 50$, $L_p/d_p = 10$, $d_r/d_p = 3$, $\lambda^r = 0.4$).

Figure 19: Variation of contact pressure ($p_r^* = F_r/q$) with normalized distance from the center of raft $R^* = r/d_p$ –effect of comparative strengthening, K_p, of GP and comparative size of raft, d_r/d_p, on partially strengthened GP–raft foundation ($L_p/d_p = 10$, $\mu^r = 4$, $\lambda^r = 0.4$).

Figure 20: Variation of percentage load w. r. t. total load with the comparative strengthening of GP, K_p – effect of comparative length of strengthening of GP, μ^r, on a partially strengthen GP–raft foundation ($L_p/d_p = 10$, $d_r/d_p = 3$, $\lambda^r = 0.4$).
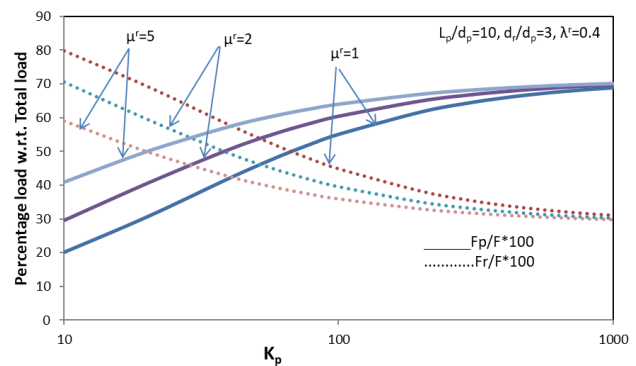
respectively. For smaller size ($d_r/d_p = 3$) of raft, the stresses are about 35.12% lower than those for the larger size ($d_r/d_p = 5$) at the edge of raft for $K_p = 100$. The magnitude of normal stresses on raft decreases with increase in the strengthening of GP.

Fig.20 shows the deviation of percentage pile load, (F_p/F) ×100, and raft load, (F_r/F) ×100, with comparative strengthening, K_p, of GP with the influence of strengthening factor, μ^r, on a partially strengthen granular piled raft for $L_p/d_p = 10$, $d_r/d_p = 3$, $\lambda^r = 0.4$. As can be expected, the percentage load of GP rises with increases of comparativestrengthening factor, μ^r, and vice versa raft load decreases. With the increase in strengthening factor $\mu^r = 1$–5, the percentage load sharing by pile is increased from 20 to 41.

Variation of percentage pile load, (F_p/F) ×100, and raft load, (F_r/F) × 100, with comparative stiffness, K_p, with the influence of comparative size of raft, d_r/d_p, on a GP raft for

$L_p/d_p = 10$, $\mu^r = 4$, $\lambda^r = 0.4$ is shown in Fig.21. The percentage load of GP decreases with the increase of the comparative size of raft, d_r/d_p, and vice versa raft load increases. As the size of raft increases, the load on raft increases.

The variation of percentage raft load, (F_r/F) × 100, with comparative strengthening of GP, K_p, is shown in Fig. 22 with the effect of the comparativelength of strengthening, λ^r, on a partially strengthened granular piled raft. The percentage raft load decreases with the rise in comparativelength of strengthening, λ^r. For $L_p/d_p = 10$, $d_r/d_p = 3$, $\mu^r = 4$, and $\lambda^r = 0.2$, 0.3, and 0.4, the values of percentage raft load decrease to 66, 63, and 61 correspondingly. The percentage raft load decreases from 66 to 61 for an increase in comparativelength of strengthening, λ^r, from 0.2 to 0.4.
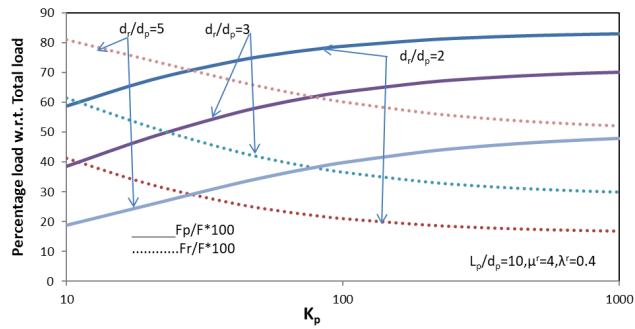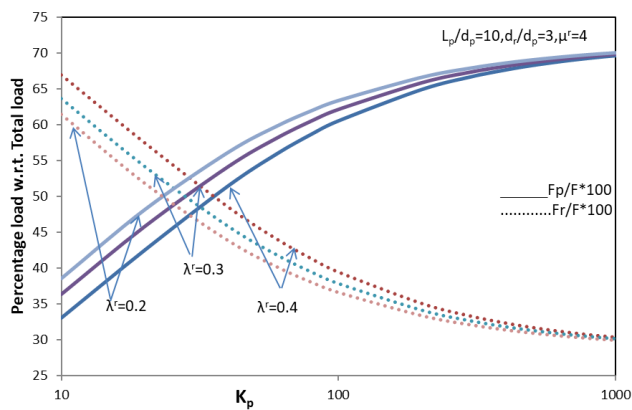
Figure 21: Variation of percentage load w. r. t. total load with the comparative strengthening of GP, K_p– effect of comparative length of GP, d_r/d_p, on a partially strengthen GP–raft foundation (L_p/d_p=10,μ^r=4,λ^r=0.4).

Figure 22: Variation of percentage load w. r. t. total load with the comparative strengthening of GP, K_p– effect of comparative length of strengthening of GP, λ^r, on a partially strengthen GP–raft foundation (L_p/d_p=10, d_r/d_p=3,μ^r=4).

5 Conclusions

Based on the finite difference technique and elastic continuum approach, new pile displacement matrix is formulated in current study. The following conclusions are drawn from this study:

- The differences in the values of SIF, i_p, obtained from the two analyses with and without radial compatibility of displacement are in the range of 1–1.5%. Thus, the consideration of radial displacement compatibility of GP in the analysis does not influence the SIF significantly.
- The decrease in the SIF with the increase of strengthening factor, μ^r, and comparative length of strengthening from top of GP, λ^r. Decrease in the SIF from μ = 1 to 5 is about 13.83% and from μ = 5 to 10 is only 4% for L/d=10, K_p = 10, D/d = 3, and λ = 0.4 which

implies that the effect is more pronounced in the range of stiffness factor μ =1–5. Further strengthening of GP in the top portion does not make a significantchange in the settlement reduction.

- The radial displacement impact factor, i_r, reduces with increasing strengthening parameters, μ^r and λ^r, thus producing the beneficial effect of strengthening, which means reducing the bulging in terms of radial displacement impact factor, i_r, in top portion of GP. Maximum radial displacement is observed in (0–3) L_p length of GP.
- The shear stresses along GP–soil interface are negative in its top region due to influence of normal stresses transferred by the raft, i.e., an effect similar to down-drag for partially strengthened granular piled raft improved along the GP. Due to strengthening in the upper portion of GP, shear stresses increase along the pile length.
- Normalized radial stresses tendto increase with the strengthening of GP. Radial stresses tend to decrease in upper portion with the size of raft in upper portion and increase in lower part of GP because of higher distance of raft edge stresses.
- The percentage reduction in the contact pressure at the raft–soil interface in comparison to the value of a solid raft is about 14% near the edge of raft for L_p/d_p = 10, d_r/d_p = 3, μ^r = 10, and K_p = 50.
- The percentage load transferred to the pile increases with the increase in strengthening parameters and comparative strengthening of GP, K_p, and vice versa percentage raft load decreases as it reflects true behavior of piled raft foundation system.

References

[1] Burland, J. B. (1977). Behaviour of foundations and structures on soft ground. *Proc. 9th ICSMFE, 1977*, *2*, 495-546.

[2] Poulos, H. G. (1968). Analysis of the settlement of pile groups. *Geotechnique*, *18*(4), 449-471.

[3] Randolph, M. F. (1983). Design of Piled Raft Foundations. Cambridge University. *Eng. Depart. Research Report, Soils TR143, Cambridge*.

[4] Huang, M., Liang, F., & Li, Z. (2007). Recent advances in the analysis of pile foundation in China. In Advances in deep foundations (pp. 127-136). CRC Press.

[5] Poulos, H.G. (2001). Piled raft foundations: design and applications. *Geotechnique*, *51*(2), 95-113.

[6] Liang, F. Y., Chen, L. Z., & Shi, X. G. (2003). Numerical analysis of composite piled raft with cushion subjected to vertical load. *Computers and Geotechnics*, *30*(6), 443-453.

[7] Liang, F., Li, J., & Chen, L. (2006). Optimization of composite piled raft foundation with varied rigidity of cushion.

In *Foundation Analysis and Design: Innovative Methods* (pp. 29-34).

[8] Eslami, A., & Malekshah, S. S. (2011). Analysis of non-connected piled raft foundations (NCPRF) with cushion by finite element method. *Computational Methods in Civil Engineering*, *2*(2).

[9] Tradigo, F., Pisanò, F., Di Prisco, C., &Mussi, A. (2015). Non-linear soil–structure interaction in disconnected piled raft foundations. *Computers and Geotechnics*, *63*, 121-134.

[10] Tradigo, F., Pisanò, F., & di Prisco, C. (2016). On the use of embedded pile elements for the numerical analysis of disconnected piled rafts. *Computers and Geotechnics*, *72*, 89-99.

[11] Sharma, V. J., Vasanvala, S. A., & Solanki, C. H. (2014). Behaviour of load-bearing components of a cushioned composite piled raft foundation under axial loading. *Slovak Journal of Civil Engineering*, *22*(4), 25-34.

[12] Eid, H. T., &Shehada, A. A. (2015). Estimating the elastic settlement of piled foundations on rock. *International Journal of Geomechanics*, *15*(3), 04014059.

[13] Huang, M., Liang, F., & Jiang, J. (2011). A simplified nonlinear analysis method for piled raft foundation in layered soils under vertical loading. *Computers and Geotechnics*, *38*(7), 875-882.

[14] Kuwabara, F. (1989). An elastic analysis for piled raft foundations in a homogeneous soil. *Soils and foundations*, *29*(1), 82-92.

[15] Lee, S., & Moon, J. S. (2017). Effect of interactions between piled raft components and soil on behavior of piled raft foundation. *KSCE Journal of Civil Engineering*, *21*(1), 243-252.

[16] Luo, R., Yang, M., & Li, W. (2018). Normalized settlement of piled raft in homogeneous clay. *Computers and Geotechnics*, *103*, 165-178.

[17] Maharaj, D. K., & Gandhi, S. R. (2004). Non-linear finite element analysis of piled-raft foundations. *Proceedings of the Institution of Civil Engineers-Geotechnical Engineering*, *157*(3), 107-113.

[18] Shen, W. Y., Chow, Y. K., & Yong, K. Y. (2000). A variational approach for the analysis of pile group–pile cap interaction. *Geotechnique*, *50*(4), 349-357.

[19]Mindlin, R. D. (1936). Force at a point in the interior of a semi-infinite solid. *physics*, *7*(5), 195-202.

[20] Sharma, J. K. (1999). *Analysis and settlement of granular pile (s)-single, in group and with raft* (Doctoral dissertation, Ph. D. Thesis, IIT, Kanpur, 408).

[21] Madhav, M. R., Sharma, J. K., & Sivakumar, V. (2009). Settlement of and load distribution in a granular piled raft. *Geomechanics and Engineering*, *1*(1), 97-112.